Bifurcation-enhanced ultrahigh sensitivity of a buckled cantilever

Sangmin An[a,1], Bongsu Kim[a], Soyoung Kwon[a], Geol Moon[b], Manhee Lee[c], and Wonho Jhe[a,1]

[a]Center for Nano-Liquid, Department of Physics and Astronomy, Seoul National University, Seoul 08826, Republic of Korea; [b]Department of Physics, Chonnam National University, Chonnam 61186, Republic of Korea; and [c]Department of Physics, Chungbuk National University, Chungbuk 28644, Republic of Korea

Edited by David A. Weitz, Harvard University, Cambridge, MA, and approved February 11, 2018 (received for review September 12, 2017)

Buckling, first introduced by Euler in 1744 [Euler L (1744) *Opera Omnia I* 24:231], a sudden mechanical sideways deflection of a structural member under compressive stress, represents a bifurcation in the solution to the equations of static equilibrium. Although it has been investigated in diverse research areas, such a common nonlinear phenomenon may be useful to devise a unique mechanical sensor that addresses the still-challenging features, such as the enhanced sensitivity and polarization-dependent detection capability. We demonstrate the bifurcation-enhanced sensitive measurement of mechanical vibrations using the nonlinear buckled cantilever tip in ambient conditions. The cantilever, initially buckled with its tip pinned, flips its buckling near the bifurcation point (BP), where the buckled tip becomes softened. The enhanced mechanical sensitivity results from the increasing fluctuations, unlike the typical linear sensors, which facilitate the noise-induced buckling-to-flipping transition of the softened cantilever. This allows the in situ continuous or repeated single-shot detection of the surface acoustic waves of different polarizations without any noticeable wear of the tip. We obtained the sensitivity above 10^6 V(m/s)$^{-1}$, a 1,000-fold enhancement over the conventional seismometers. Our results lead to development of mechanical sensors of high sensitivity, reproducibility, and durability, which may be applied to detect, e.g., the directional surface waves on the laboratory as well as the geological scale.

bifurcation | nonlinear force sensor | atomic force microscopy | buckling | seismometer

Mechanical sensors play key roles in fundamental measurements and practical applications, such as the force (1) or pressure sensor (2), the accelerometer (3), and inertial sensors or seismometers (4). Although various schemes of sensors (5, 6) have been developed with improved sensitivities (7), there still exists much demand for novel devices that use the unexplored mechanical mechanisms to address difficult problems. One of the nonlinear mechanical phenomena useful for such sensors is buckling (8), an instability that leads to a flexural fracture under a high load. It has been widely discussed in regard to, for example, bending and buckling of carbon nanotubes (9), compressibility of living cells (10), and buckling of various materials (11, 12). In particular, nonlinear complex behaviors have been studied in such processes as elastohydrodynamic instabilities (13) and buckling of elastic filaments (14). Moreover, recent studies have shown that buckling instability (or asymmetric buckling mode) enhances the sensitivity of the hair-cell buckling-tip links (15) and the biomimetic force sensor mimicking the auditory hair cell (16). Therefore, it would be worthwhile to investigate whether the buckling nonlinearity can be applicable to challenging devices, such as the seismometer (17) operating on the zero-length spring (18) or the force balance method (19), whose linearity requires advances in the lower noise for the higher sensitivity essential for early prediction of earthquakes (20).

Here, we realize the bifurcation-enhanced mechanical sensitivity of the buckled cantilever, combined with the quartz tuning-fork–based atomic force microscope (QTF-AFM) (Fig. 1*A*) (21–23). The buckled tip, when softened as the flexural stress is released by the accumulated external shear forces near the bifurcation point (BP), enhances its noise-induced flip due to the increased fluctuations. As a result, the system enables the highly sensitive and quantitative dynamic force measurement, which leads to the continuous and simultaneous detection of the polarization-dependent surface acoustic waves on the laboratory scale. One may picture the buckled oscillator in terms of a bifurcation that leads to two equilibrium states as described by the double-well potential (Fig. 1*B*). Driving toward the BP by the external forces corresponds to biasing the potential, so that the local potential minimum that represents the buckling becomes shallower and vanishes, resulting in the flip of the tip. The QTF–cantilever tip coupling can be qualitatively considered as an interaction between two harmonic oscillators (frequencies of ω_f and ω_t) although the detailed bifurcation dynamics are beyond the simple single-mode analysis. Interestingly, the buckling-to-flipping transition of the softened tip (i.e., $\omega_t \approx 0$) is similar to the stick–slip friction of a sharp AFM tip except that the tip is pinned on the substrate during the transition.

Results and Discussion

Simple Single-Mode Analysis of the QTF–Cantilever Tip Coupling. We discuss the coupling of the QTF and the cantilever tip as an

Significance

This work brings together the fields of nonlinear dynamics and precision measurement, aiming to develop a highly sensitive nonlinear mechanical force sensor. We use dynamic force spectroscopy of the buckled cantilever tip in an ambient condition, which allows sensitive detection of the noise-induced flipping near the bifurcation point. Key parameters, such as the fluctuation enhancement and the activation barrier of the buckling-to-flipping transition, lead to realization of the bifurcation-enhanced sensor. We contiguously observe the buckling–flipping dynamic transition of the softened tip resulting from the competition between fluctuation and bifurcation, providing the in situ continuous sensing of the mechanical vibrations. This work not only furthers our understanding of nonlinear dynamics at the nanoscale, but also is a stepping stone toward the highly sensitive mechanical sensor.

Author contributions: S.A. and W.J. designed research; S.A. performed research; B.K., S.K., G.M., M.L., and W.J. contributed new reagents/analytic tools; S.A., B.K., M.L., and W.J. analyzed data; and S.A., M.L., and W.J. wrote the paper.

The authors declare no conflict of interest.

This article is a PNAS Direct Submission.

[1]To whom correspondence may be addressed. Email: whjhe@snu.ac.kr or jmk8755@snu.ac.kr.

This article contains supporting information online at www.pnas.org/lookup/suppl/doi:10.1073/pnas.1716067115/-/DCSupplemental.

Published online March 6, 2018.

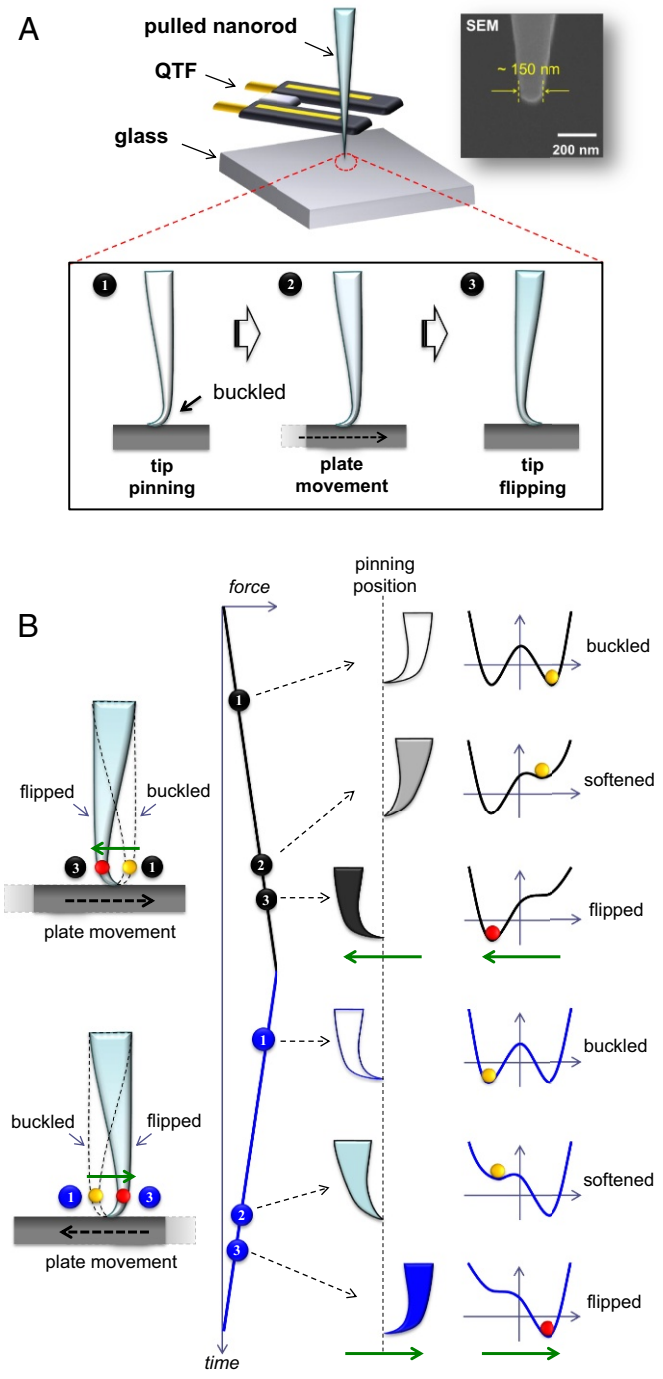

Fig. 1. Buckled tip-based nonlinear mechanical sensor. (*A*) Experimental schematics of the buckled cantilever tip that flips near the BP. The sharp tip approaches the substrate until its pinning on the surface and the subsequent buckling under the flexural stress (*1*) stays pinned during a lateral movement of the substrate, accumulating the external shear forces on the buckled tip (*2*), and makes the nonlinear fluctuation-induced abrupt flip with the buckling direction reversed (*3*). (*B*) The temporal and spatial configurations as well as the energy landscape of the bifurcation dynamics associated with the buckling–flipping transition. The buckled cantilever tip is considered to occupy initially one of the two local minima of the double-well potential (*1*), softened as the BP is approached by the increasing potential bias due to the external shear stress, lowering the potential barrier (*2*), and flipped to the opposite potential minimum, reversing its buckling direction (*3*). This forward movement of the substrate, represented by *1*–*3* positions in time (black color), is then reversed by the backward movement (blue color). Here, the yellow (red) circle in the symmetric double-well potential characterizes the buckled (flipped) tip, and thus the green arrow measures the distance between the two circles, similar to the slip length in the stick–slip friction.

interaction between two harmonic oscillators with frequencies ω_f and ω_t, respectively. If the vibrational coordinate of the QTF is x and that of the tip is q_t, one can write the coupling energy as $H_c = Cq_t x$. The full Hamiltonian before the tip is flipped by the external stress is $H = p_f^2/2m_f + p_t^2/2m_t + m_f\omega_f^2 x^2/2 + m_t\omega_t^2 q_t^2/2 + H_C$, where the effective mass of the QTF (cantilever) is m_f (m_t). The parameter C should be found from the boundary condition that the fork and the cantilever are in contact (Fig. 1*A*). Note that, in writing this condition, one has to take explicitly into account the shape of the cantilever mode at the contact as well as the shape of the QTF mode. We obtain the shift of the QTF frequency, $\omega - \omega_f \approx -C^2/\left[2m_t m_f \omega_f \left(\omega_t^2 - \omega_f^2\right)\right]$. Our estimate shows $\omega_t \gg \omega_f$, and so we can disregard ω_f^2 in the denominator. This expression is in qualitative agreement with the experimental result that a longer tip leads to a stronger frequency decrease (24), resulting in a smaller ω_t (although one should more carefully check how C depends on the parameters for quantitative analysis).

Another consequence of the coupling H_C is the extra damping of the QTF mode. It results from the coupling of the cantilever mode to other modes in the cantilever, which makes the characteristic time of the considered mode finite. Formally, one can obtain this by adding the corresponding decay rates Γ_f and Γ_t to the equations of motion of the coupled modes. This changes the effective decay rate as $\Gamma_f \to \Gamma_f + \Gamma_t C^2/\left[m_t m_f \omega_t^4\right]$ for $\omega_t \gg \omega_f$. Note that although the buckling changes the modes of the cantilever, the shifts of the frequency ω_t should not be too dramatic but vary by a factor of order 1, except in the vicinity of the bifurcation. The physical mechanism of the nonlinear transition model is presented in *Nonlinear Transition Model* and Fig. S1, describing the buckling, softening, and flipping transition for better understanding of the sensor responses. Note that the dynamics close to the BP are not described by the simple single-mode analysis: One has to take into account other modes in the tip and their interaction, including their decay. Such a full analysis is beyond the scope of this work, for which the effective elasticity of the tip (or ω_t) goes to zero and thus the model of a cantilever breaks down as the shape of the tip changes.

Buckled Tip-Based Nonlinear Mechanical Sensor. The experimental procedures for the buckling-assisted nonlinear mechanical detection in ambient conditions are as follows (Fig. 1*A*): approach of the cantilever tip (pulled quartz nanorod), contact on the substrate (Pyrex glass, 1.5 × 1.5 cm^2 area, 150 μm thickness), and gentle push until the initial buckling state of the tip is prepared (*1*); lateral movement of the glass plate in the direction against the buckled tip that is pinned on the plate (*2*); and abrupt flip of the softened tip, reversing its buckling direction, over the lowered potential barrier near the BP (*3*). Fig. 1*B* describes the schematic of the tip configuration and the energy landscape corresponding to each step from buckling to flipping during one cycle of the applied forces via a round-trip movement of the substrate. Note that although the initial buckling direction (Fig. 1*A*) can be randomly determined by the instantaneous contact force, the tip is made slightly tilted within a few degrees of angle with respect to the x axis, so that it is preferentially buckled in a specific direction due to its broken translational symmetry (25) (see *Tip and Substrate* and Fig. S2 for details). Note also that the local buckling on the tip is elastic, not of plastic deformation, as discussed in *Elasticity, Reliability, and Durability of the Buckled-Tip Sensor*.

Noise-Induced Flipping Near the BP. Dynamic force spectroscopy was performed by FM-mode QTF-based AFM (26). Fig. 2*A* presents the experimental results for the two consecutive flips of the buckled tip during the bidirectional (forward and backward) slow (50 nm/s speed) movement of the substrate. As shown, the measured QTF-frequency shift Δf (damping coefficient g')

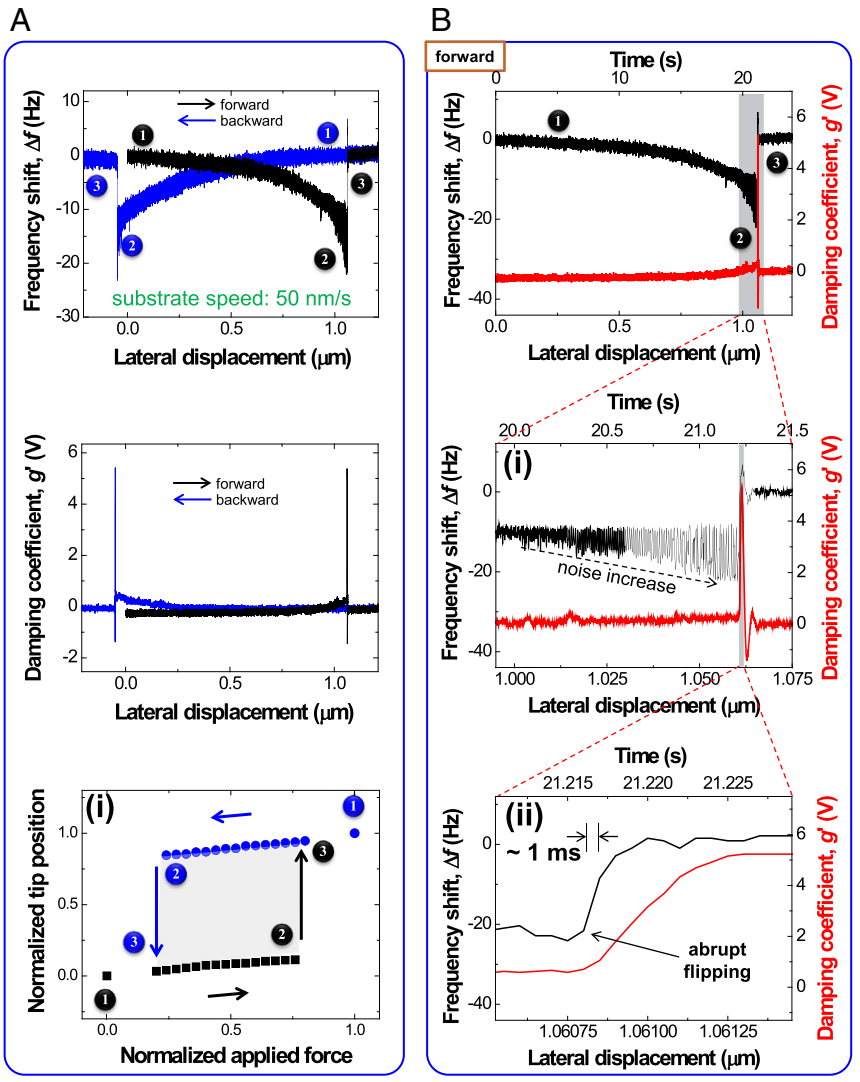

Fig. 2. Noise-induced flip near the BP. (*A*) During a lateral displacement of the substrate, the buckled tip experiences the accumulated external shear stress, releasing the flexural stress while the tip is pinned, and becomes softened and then flips. The buckling-to-flipping transition is enhanced by the increasing nonlinear fluctuations as the system approaches the BP (i.e., near position *2* here and in Fig. 1). As shown, the continuous accumulation of the forces results in the gradual decrease of the QTF frequency (Δf) and the slight increase of the damping coefficient (g') in the frequency modulation (FM)-detection mode of the QTF-AFM. The position 0.5 μm marks the center between the two flips that are apart by ∼1 μm. Note that the plate moves a distance of ∼1.25 μm in each direction, i.e., 0.25 μm beyond the flip, which informs the maximum applied force before the flip occurs. Interestingly, the applied force [normalized to the maximum force of 30 μN (= 30 N/m × 1 μm)] vs. the flip distance (normalized to the maximum separation between the two colored circles) is plotted in *A*, *i*, which exhibits the hysteresis where the position data are obtained by direct analysis of the captured optical microscope images. (*B*) Plot of Δf and g' associated with the forward movement of the plate. The gradual decrease of Δf is clearly observed during a lateral movement (at the speed of 50 nm/s for the duration of ∼22 s) over the 1-μm distance. The enhanced nonlinear fluctuations are noticeable in the narrower time window between 20 s and 21 s near the BP in *B*, *i*, as well as in *B*, *ii* where the fast time-resolved mechanical responses associated with the rapid flip (∼1 ms in 0.2 nm distance) as well as the damped oscillation (∼10 ms) are observed.

gradually and slightly decreases (increases) with the increasing applied forces and shows the sudden change, indicating the flipping. The frequency is then recovered to the initial value as the tip is buckled again. Here, the numbers *1–3* in both directions correspond to the respective steps shown in Fig. 1*B*, where the bifurcation is characterized by the double-well potential. As a force sensor, the QTF oscillator measures quantitatively the tip–QTF interaction forces while the system undergoes the nonlinear transient dynamics. In dynamic force spectroscopy of AFM, the external interaction experienced by the QTF can be decomposed into the effective elastic ($F_{\rm k}$) and damping ($F_{\rm b}$) forces, which are characterized by the effective elasticity ($k_{\rm int}$) and damping constant ($b_{\rm int}$), respectively, for small (nanoscale) oscillation of the tip (*Detection System*). The elastic force ($F_{\rm k}$) and damping force ($F_{\rm b}$), or alternatively the dissipated energy ($E_{\rm dis}$), are experimentally obtained by measuring Δf and g' of the QTF in the FM-mode operation of dynamic AFM (23, 27) (Fig. S3). $E_{\rm dis}$ also defines how much energy obtained by lateral motion can dissipate through the substrate and the air. Interestingly, the system exhibits hysteretic behavior between the two flips (Fig. 2 *A*, *i*), where each flip is represented by the green horizontal arrow in Fig. 1*B*. The length of the arrow denotes the flip distance, like the slip length in the stick–slip friction of a single-asperity AFM tip (28, 29). The area of the force–distance hysteresis equals twice the dissipated energy during one period of the forward–backward flipping processes.

The flip results from the decreasing activation energy barrier close to the BP, where the increasing fluctuations facilitate

the flipping even at small mechanical disturbances (Fig. 2*B*). Importantly, such a bifurcation-enhanced sensitivity does not dominantly come from the quality (Q)-factor increment, which is typical in the linear dynamic systems, but from the nonlinear dynamic response of the buckled tip near the BP. Here, we address the physical origin of such a bifurcation-induced sensitivity enhancement. The change Δf of the resonance frequency $f_0(=\omega_f/2\pi)$ is related to the measured quality factor Q' and damping coefficient g' by $Q/Q' = (1+\Delta f/f_0)g/g'$, where Q and g are the corresponding initial values in the FM-mode operation. Since $\Delta f \ll f_0$ and $g'/g > 1$ as the system approaches the BP, Q' actually decreases below Q, which indicates the bifurcation-enhanced sensitivity is achieved even at the lowered Q value. Note that the Q value is associated with the damping of the system, which is another important parameter that determines the energy dissipation in the system and controls details of the nonlinear transition after flipping (30). In addition, the high-Q tip experiences a high damping when the tip flips and dissipates substantial elastic energy stored in the system just before its flip, and thus it is unlikely for the buckled tip to settle back into the potential well it was nudged out of.

Fig. 2*B* presents only the forward-direction data with detailed views of the flip-occurring transient (gray) region. We observe the increasing fluctuations in Δf toward the BP (Fig. 2 *B*, *i*), which are proportional (31) to $1/\sqrt{\omega_t}$, as they are induced by the enhanced mechanical instability of the increasingly softened buckled tip. The frequency fluctuations (Fig. S4) are characterized by the SDs that are calculated for the measured data of Δf during plate movement. As shown, while the QTF frequency is decreased by ∼20 Hz during the overall ∼1-μm displacement, the SD increases from ∼1 Hz up to ∼10 Hz, and especially it drastically increases in the region from 0.96 μm to 1.06 μm. Another important result is that the response time during the flip is measured as ∼1 ms (Fig. 2 *B*, *ii*), which reflects only the AFM-system bandwidth (26), indicating the flip time can be made farther below 1 ms despite the slight increase in g'.

Velocity Dependence of the Nonlinear Dynamic Buckling-to-Flipping Transition. To characterize the nonlinear dynamics of the noise-induced flip, we have investigated the dependence of the buckling-based mechanical sensitivity on the velocity of the moving substrate. Fig. 3*A* (Fig. 3*B*) plots the interaction forces, F_k and F_b, vs. the displacement (time) for various speeds from 1.5 μm/s to 35 μm/s, which are derived from the measured Δf and g' in Fig. S5 (Fig. S6). As shown in Fig. 3*A*, whereas the lateral distance that the substrate travels between the two flips decreases with speed, the bifurcation region becomes broadened at the high speed so that the buckled tip can start sensing the interactions away from the flipping point. In general, when the control or excitation parameters are not stationary but vary in a continuous manner, the bifurcation or loss of stability (so-called saddle-node bifurcation) occurs away from the point at which the static bifurcation occurs (32), which is also consistently observed in our system. Since such parameters are nonstationary and vary slowly with time, various physical and engineering systems have shown continuous dynamical behaviors such as sudden jumps (33) and oscillations around the static equilibrium points (34). Interestingly, the sensitivity, especially in F_k, is relatively high near the BP even at the very low speed, and thus the force measurements can be made either close to or away from the BP (i.e., independent of speed). Moreover, the fluctuations are larger at the lower speed, at which the noise-induced flip is expected to

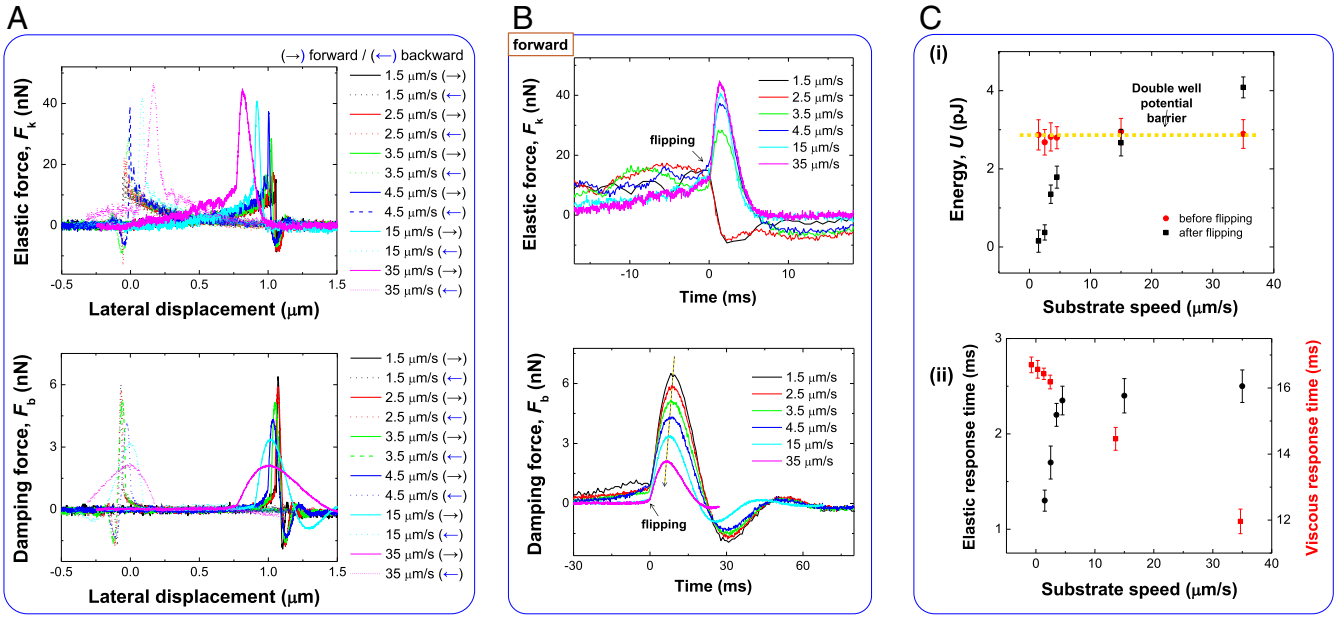

Fig. 3. Velocity dependence of the buckling–flipping transition. (*A*) The spatial behaviors of F_k and F_b are presented for various speeds from 1.5 μm/s to 35 μm/s in the forward and backward directions between the two consecutive flips. We find that while both F_k and F_b rapidly change near the flipping region, the corresponding bifurcation region is broadened with speed. At low speed, the interflip distance is about 1 μm and the associated force sensitivity is high enough to be useful for a mechanical sensor even at zero speed (i.e., even in the stationary case). Here, the 0.5-μm position represents the midposition of the substrate between the bidirectional flips. (*B*) The temporal variations of F_k and F_b are provided, which replot the spatial data of *A* with respect to the travel time of the substrate. As the speed increases, we observe gradual suppression of the increasing fluctuations of F_k near the BP, which indicates the sensor has the unique noise-induced characteristics of the nonlinear oscillator that allow the higher sensitivity at the lower speed. Note that the time origins of the data are arbitrarily offset just for convenient comparison of the temporal behaviors near the BP. (*C*) Calculated values of the symmetric double-well potential barrier before and after the flip, as well as the temporal properties of the elastic and viscous response. As shown in *C*, *i*, the central barrier energy is estimated as ∼2.9 pJ, obtained by summing the accumulated energy for each speed up to the flipping point, which is found to be independent of the plate speed. At the lower speed, in particular, the system exhibits in *C*, *ii* higher temporal sensitivity with the instantaneous elastic response time of the bandwidth-limited ∼1 ms, whereas the viscous response time increases at the lower speed.

be more favorable. On the other hand, Fig. 3*B* shows that the temporal response of F_k falls sharply (saturates) at the low (high) speed, whereas that of F_b behaves oppositely with a fast (slow) response at the high (low) speed. At low speed (<2.5 μm/s), the tip stays longer in the bifurcation region and the accumulated stress is dissipated sufficiently enough for the repeated (or continuous) detection of the flipping, and thus F_k shows rapid flip without any extra energy left. At high speed (>3.5 μm/s), however, the shorter stay near bifurcation leads to less dissipation (F_b), and the extra elastic energy of F_k increases noticeably with speed beyond the activation threshold (Fig. 3 *C*, *i*). The data in Fig. 3*B* are summarized in Fig. 3 *C*, *ii*, which shows that F_k at the low (or even zero) speed provides the fastest response (~1 ms at 1.5 μm/s).

The energy barrier of the symmetric double-well potential for the buckled oscillator (Fig. 1*B*) is $\sim 2.9 \times 10^{-12}$ J, which is obtained by adding the mechanical energy of the system up to the flipping point (Fig. 3 *C*, *i*). As expected, this potential barrier is constant and independent of the substrate speed. In particular, the activation energy needed for the softened tip to flip is $\sim 3.8 \times 10^{-16}$ J, that is, the elastic energy at the distance (~5 nm) having appreciable fluctuations just before the flipping point, which is also speed independent because of the constant effective stiffness (~30 N/m). Importantly, the results in Fig. 3 *C*, *i* and *ii* suggest that the higher sensitivity in the spatial as well as temporal response is obtained at the lower speed or even when the system is stationary at a distance from the BP, which allows the in situ continuous sensing, as demonstrated in Fig. 4. We emphasize again that the bifurcation-enhanced sensitivity is possible because while the activation energy is almost constant and independent of the speed, the larger fluctuations (Fig. 2) and thus the higher sensitivity (Fig. 3), contrary to the linear sensors, are available at the lower speed, which accelerates the noise-induced buckling–flipping transition near the BP.

Buckling-Based Sensitive Detection of the Surface Acoustic Waves. The buckling-based sensor allows the sensitive, simultaneous detection of the polarization-dependent surface acoustic waves, which modulate the vibration frequency ω_t due to the acoustic compression in the tip. Because the tip is slightly tilted, the modulation occurs for both the P wave and the L wave, excited by the perpendicular and lateral mechanical resonances of the system, respectively. To demonstrate quantitatively this unique capability, we place the tip either in the midst of the noise increment (region 1) or in the vicinity of the BP (region 2) in Fig. 4*A*. In region 1 that is relatively away from the BP, the still-appreciable fluctuations allow the in situ continuous nondestructive sensing without a tip flip (Fig. 4*B*), whereas the highly sensitive single-shot detection accompanying the single flip can be made in region 2 (Fig. 4*C*). The external mechanical perturbations in region 1 can be excited by, e.g., a coin (mass of ~5.5 g) that is dropped nearby above the optical table at various release heights from 5 cm to 25 cm (Fig. S7*A*). We plot the increase of F_k and F_b (Fig. 4*B*) as well as E_{dis} (Fig. S7*D*) vs. the drop

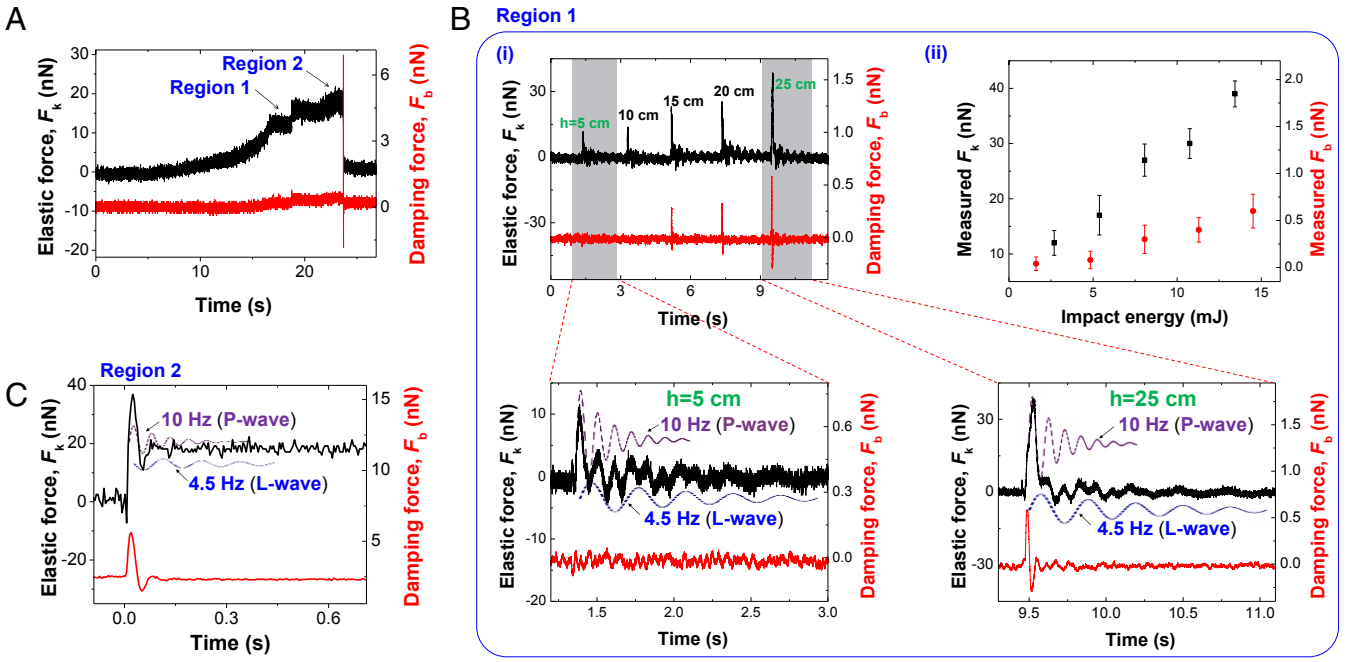

Fig. 4. Detection of the polarization-dependent surface acoustic waves. (*A*) Two modes of operation as the mechanical sensor are demonstrated. The buckled tip can be configured either for the in situ continuous but less sensitive detection of F_k and F_b without the flip slightly away (~20 nm) from the BP (region 1) or for the repeated single-flip but more sensitive detection in the vicinity (<10 nm) of the BP (region 2). (*B*) Continuous detection of F_k and F_b excited by the mechanical vibrations resulting from the nearby (~20 cm away) impact of a coin (mass of ~5.5 g) dropped at various release heights from 5 cm to 25 cm. We find that the two polarization-dependent mechanical waves were simultaneously detected at the differing oscillation frequencies, P wave (10 Hz) and L wave (4.5 Hz), as shown in *B*, *i* and *ii*, *Lower*. The bigger impact and thus the larger F_k values were measured, while no sizable signal of F_b was detected when the coin was release at the height of 5 cm, indicating that F_b is relatively less sensitive to the weak mechanical disturbances. In *B*, *ii*, the measured forces are plotted with respect to the impact energy for the coin drop. Note that most of the coin's kinetic energy (2.7×10^{-3} J and 1.4×10^{-2} J for the 5-cm and 25-cm heights, respectively) is absorbed by the system (mass of ~15 kg), while the remaining energy exerts the forces onto the tip, as manifested by the measured F_k and F_b. (*C*) Single-shot detection of the weak surface acoustic waves, accompanied by the single flip of the buckled tip at a fixed position close to the BP (region 2). Note that the flipped tip immediately restores its newly buckled state, ready for the next single-shot measurement, so that the repeated (virtually continuous) single-shot sensing can be realized with no appreciable tip wear (*Elasticity, Reliability, and Durability of the Buckled-Tip Sensor*). Here, the surface acoustic waves of differing frequencies produce the mechanical vibrations propagating at unequal speeds, as in the seismic primary wave and secondary wave. Note that all of the temporal curves here are given an arbitrary vertical offset just for convenience of comparison.

height, obtained by the calculated $k_{\rm int}$ and $b_{\rm int}$ (Fig. S7*C*) for the measured Δf and g' (Fig. S7*B*). As shown, the two independent, damped mechanical waves oscillating at ∼10 Hz (P wave) and ∼4.5 Hz (L wave) were simultaneously detected. Moreover, a gentle tap on the table also produces the polarization-dependent waves in region 1: both the P and L waves by a perpendicular tap, whereas only the L wave by a lateral tap (Fig. S8).

Remarkably, in the more sensitive region 2, a minute interaction energy of $\sim 10^{-15}$ J (i.e., elastic energy at ∼10 nm from the BP) above the activation threshold ($\sim 3.8\times 10^{-16}$ J) is expected to trigger the bifurcation-enhanced flip (Fig. 4*C*). For such a faint perturbation, the buckled tip flips and provides a sensitive detection of the P wave (∼10 Hz), whereas the L-wave (∼4.5 Hz) response is suppressed because the tip flips onto the stable state. Note that while such a noise-induced detection near the BP can occur at any moment, the flipped tip can immediately reset itself, ready for the next single-shot measurement by automatic control of the plate motion, which allows the repeated (or continuous) monitoring of the weak, low-frequency surface acoustic waves, such as the large-scale mechanical vibrations. In addition, one can expect to reach the minimum detectable force sensitivity of $\sim 10^{-14}$ N (*Minimum Detectable Force*) if the buckled tip is parked near the BP, which performs uniquely compared with the typical linear sensors (35). We now discuss the sensitivity of the mechanical sensors, which is generally measured via the gauge factor, the ratio of change in the electrical resistance to the mechanical strain. For example, the seismometers are characterized in units of $\mathrm{V(m/s)}^{-1}$ and the typical value (36) is $\sim 2\times 10^{3}$ $\mathrm{V(m/s)}^{-1}$. However, we obtain $\sim 10^{6}$ $\mathrm{V(m/s)}^{-1}$ in region 1 and $\sim 4\times 10^{6}$ $\mathrm{V(m/s)}^{-1}$ in region 2, as derived by using the output voltage of the sensor and the calculated wave-propagation speed. Finally, we also have addressed the mechanical stability of the buckled-tip sensor by checking the resonance curves of the QTF before and after (*i*) buckling as well as (*ii*) continuous flips (*Elasticity, Reliability, and Durability of the Buckled-Tip Sensor*).

In conclusion, using the nonlinear dynamic buckled tip, we have demonstrated the bifurcation-enhanced sensitive, continuous in situ detection of the weak mechanical vibrations having different polarizations in ambient conditions. Importantly, the larger fluctuations produce the higher sensitivity, unlike the linear sensors that demand lower noise, which may be associated with stochastic resonance. Our results are useful for practical applications, such as the seismic sensor that needs further development in detecting the primary and secondary waves, or even the faint precursor wave, which is indeed expected to be feasible considering other similar uses of the QTFs (16). Moreover, one can expect to control automatically the tip's dynamic configuration near the BP ready for the durable sensitive detection of the surface acoustic waves, using the systematic data analysis based on our quantitative sensing capabilities.

ACKNOWLEDGMENTS. This work was supported by National Research Foundation of Korea (NRF) grants funded by the Korean government (Ministry of Science & Information and Communication Technology) (2016R1A3B1908660 and 2017R1C1B5076655), the Basic Science Research Program through the NRF funded by the Ministry of Education (2017R1A6A3A11033301), and in part by the research grant of the Chungbuk National University in 2017.

1. Autumn K, et al. (2000) Adhesive force of a single gecko foot-hair. *Nature* 405: 681–685.
2. Someya T, et al. (2004) Large-area, flexible pressure sensor matrix with organic field-effect transistors for artificial skin applications. *Proc Natl Acad Sci USA* 101:9966–9970.
3. Boser BE, Howe RT (1996) Surface micromachined accelerometers. *IEEE J Solid-State Circuits* 31:366–375.
4. Brune J (1970) Tectonic stress and the spectra of seismic shear waves from earthquakes. *J Geophys Res* 75:4997–5009.
5. Lammerink TSJ, Tas NR, Elwenspoek M, Fluitman JHJ (1993) Micro-liquid flow sensor. *Sens Actuators A* 37-38:45–50.
6. Kumar D, et al. (2011) Bifurcation-based mass sensing using piezoelectrically-actuated microcantilevers. *Appl Phys Lett* 98:153510.
7. Kang D, et al. (2014) Ultrasensitive mechanical crack-based sensor inspired by the spider sensory system. *Nature* 516:222–226.
8. Varelis D, Saravanos DA (2002) Nonlinear coupled mechanics and initial buckling of composite plates with piezoelectric actuators and sensors. *Smart Mater Struct* 11:330.
9. Falvo MR, et al. (1997) Bending and buckling of carbon nanotubes under large strain. *Nature* 389:582–584.
10. Chicurel ME, Chen CS, Ingber DE (1998) Cellular control lies in the balance of forces. *Curr Opin Cell Biol* 10:232–239.
11. Kim J, Hanna JA, Byun M, Santangelo CD, Hayward RC (2012) Designing responsive buckled surfaces by halftone gel lithography. *Science* 335:1201–1205.
12. Yu C, Wang Z, Yu H, Jiang H (2009) A stretchable temperature sensor based on elastically buckled thin film devices on elastomeric substrates. *Appl Phys Lett* 95:141912.
13. Swan JW, Vasquez PA, Furst EM (2014) Buckling instability of self-assembled colloidal columns. *Phys Rev Lett* 113:138301.
14. Becker LE, Shelley MJ (2001) Instability of elastic filaments in shear flow yields first-normal-stress differences. *Phys Rev Lett* 87:198301.
15. Kachar B, Parakkal M, Kurc M, Zhao Y, Gillespie PG (2000) High-resolution structure of hair-cell tip links. *Proc Natl Acad Sci USA* 97:13336–13341.
16. Song T, Park HC, Ahn KH (2009) Proposal for high sensitivity force sensor inspired by auditory hair cells. *Appl Phys Lett* 95:013702.
17. Hsiao KH, Yan HS (2009) Structural synthesis of Zhang Heng's seismoscope with cam-linkage mechanisms. *J Adv Mech Des Syst* 3:179–190.
18. Wielandt E, Streckeisen G (1982) The leaf-spring seismometer: Design and performance. *Bull Seism Soc Am* 72:2349–2367.
19. Stuart-Watson D, Tapson J (2004) Simple force balance accelerometer/seismometer based on a tuning fork displacement sensor. *Rev Sci Instrum* 75:3045.
20. Given DD, et al. (2014) Technical implementation plan for the shake alert production system: An earthquake early warning system for the west coast of the United States. *US Geol Surv Open-File Rep* 2014-1097:1–25.
21. Giessibl FJ (1995) Atomic resolution of the silicon (111)-(7x7) surface by atomic force microscopy. *Science* 267:68–71.
22. Lee M, Jhe W (2006) General theory of amplitude-modulation atomic force microscopy. *Phys Rev Lett* 97:036104.
23. Lee M, Sung B, Hashemi N, Jhe W (2006) Study of a nanoscale water cluster by atomic force microscopy. *Faraday Discuss* 141:415–421.
24. An S, et al. (2014) Nanopipette combined with quartz tuning fork-atomic force microscope for force spectroscopy/microscopy and liquid delivery-based nanofabrication. *Rev Sci Instrum* 85:033702.
25. An S, et al. (2014) Position-resolved surface characterization and nanofabrication using an optical microscope combined with a nanopipette/quartz tuning fork atomic force microscope. *Nano-Micro Lett* 6:70–79.
26. An S, et al. (2012) Quartz tuning fork-based frequency modulation atomic force spectroscopy and microscopy with all digital phase-locked loop. *Rev Sci Instrum* 83:113705.
27. An S, et al. (2012) Mechanical properties of the nanoscale molecular cluster of water meniscus by high-precision frequency modulation atomic force spectroscopy. *Appl Phys Lett* 101:053114.
28. Bhushan B, Israelachvili JN, Landman U (1994) Nanotribology: Friction, wear and lubrication at the atomic scale. *Nature* 374:607–616.
29. Mo Y, Turner KT, Szlufarska I (2009) Friction laws at the nanoscale. *Nature* 457:1116–1119.
30. Conley WG, Krousgrill CM, Raman A (2008) Stick-slip motions in the friction force microscope: Effects of tip compliance. *Tribol Lett* 29:23–32.
31. Dykman MI, Krivoglaz MA (1980) Fluctuations in nonlinear systems near bifurcations corresponding to the appearance of new stable states. *Physica A* 104:480–494.
32. Raman A, Bajaj AK, Davies P (1996) On the slow transition across instabilities in nonlinear dissipative systems. *J Sound Vib* 192:835–865.
33. Haberman R (1979) Slowly varying jump and transition phenomena associated with algebraic bifurcation problems. *SIAM J Appl Math* 37:69–106.
34. Erneux T, Mandel P (1986) Imperfect bifurcation with a slowly-varying control parameter. *SIAM J Appl Math* 46:1–15.
35. Li M, Tang HX, Roukes ML (2007) Ultra-sensitive NEMS-based cantilevers for sensing, scanned probe and very high-frequency applications. *Nat Nanotechnol* 2:114–120.
36. Havskov J, Alguacil G (2004) *Instrumentation in Earthquake Seismology* (Springer, New York).